Research Article | Vol. 27, No. 23 | 11 Nov 2019 | OPTICS EXPRESS 34192
Optics EXPRESS

81 supra-THz beams generated by a Fourier grating and a quantum cascade laser

YUNER GAN,[1,2,7] BEHNAM MIRZAEI,[1,3] JOSE R. G. SILVA,[1,2] ALI KHALATPOUR,[4] QING HU,[4] CHRISTOPHER GROPPI,[5] JOSE V. SILES,[6] FLORIS VAN DER TAK,[1,2] AND JIAN-RONG GAO[1,3,8]

[1]*SRON Netherlands Institute for Space Research, Groningen/Utrecht, The Netherlands*
[2]*Kapteyn Astronomical Institute, University of Groningen, 9747 AD, Groningen, The Netherlands*
[3]*Faculty of Applied Science, Delft University of Technology, Delft, The Netherlands*
[4]*Department of Electrical Engineering and Computer Science, Massachusetts Institute of Technology, Cambridge, MA 02139, USA*
[5]*School of Earth and Space Exploration, Arizona State University, AZ, USA*
[6]*NASA Jet Propulsion Laboratory, Pasadena, CA, USA*
[7]*y.n.gan@sron.nl*
[8]*j.r.gao@sron.nl*

Abstract: Large heterodyne receiver arrays (~100 pixel) allow astronomical instrumentations to map more area within limited space mission lifetime. One challenge is to generate multiple local oscillator (LO) beams. Here, we succeeded in generating 81 beams at 3.86 THz by combining a reflective, metallic Fourier grating with an unidirectional antenna coupled 3rd-order distributed feedback (DFB) quantum cascade laser (QCL). We have measured the diffracted 81 beams by scanning a single pyroelectric detector at a plane, which is in the far field for the diffraction beams. The measured output beam pattern agrees well with a simulated result from COMSOL Multiphysics, with respect to the angular distribution and power distribution among the 81 beams. We also derived the diffraction efficiency to be 94 ± 3%, which is very close to what was simulated for a manufactured Fourier grating (97%). For an array of equal superconducting hot electron bolometer mixers, 64 out of 81 beams can pump the HEB mixers with similar power, resulting in receiver sensitivities within 10%. Such a combination of a Fourier grating and a QCL can create an LO with 100 beams or more, enabling a new generation of large heterodyne arrays for astronomical instrumentation.

1. Introduction

Radiation at terahertz (THz) frequencies, broadly defined as the 0.3 THz – 10 THz range, has attracted wide interest for applications in astronomical instrumentation, biomedicine, plasma diagnostics and homeland security [1]. Compared to THz direct detection techniques, heterodyne detection, combining a mixer with a local oscillator (LO) to convert a THz frequency radiation line to a lower frequency ~GHz signal, has the advantages of extremely high spectral resolution together with a quantum noise limited sensitivity. These characteristics make heterodyne detection a powerful technique in astronomical instrumentations to resolve the velocity information from molecular rotational lines and atomic fine structure lines at THz frequencies in the interstellar medium (ISM). For examples, velocity-resolved large-scale images in the fine-structure line of ionized carbon [CII] at 1.9 THz, observed by a 14-pixel heterodyne array receiver on the Stratospheric Observatory For Infrared Astronomy (SOFIA) [2], provide an observational diagnostic for the radiative energy input and the dynamics of the interstellar medium around massive stars [3]. The [CII] spectral line from the Stratospheric THz Observatory 2 (STO2), which is equipped with a 2-pixel heterodyne array, is compared with other fine structure lines to investigate the kinematics of the Trumpler 14 region in the Carina Nebula Complex [4].

#374660 https://doi.org/10.1364/OE.27.034192
Journal © 2019 Received 7 Aug 2019; accepted 25 Aug 2019; published 7 Nov 2019

Optics EXPRESS

In the applications for homeland security, heterodyne techniques can be useful for both active imaging and passive imaging system [5]. A heterodyne imaging system is attractive because such a system detects not only the intensity, but also the phase, making the detection more decisive than the direct detection [6]. Both astronomical and homeland security applications will benefit from a heterodyne array to increase the imaging speed or observation efficiency [7]. Currently, due to the high power consumption in the backend of a heterodyne receiver, including low noise amplifiers and spectrometers, and the needs of the local oscillator (LO) array [8], the practical heterodyne receivers operating at supra-THz (> 1 THz) are limited to an order of 10 pixels. With recent advances in backend technology, involving low-noise-amplifiers [9] and CMOS digital spectrometers [10], both of which have demonstrated impressively low power consumptions, one can envision large heterodyne arrays, for example, 100 pixels or more, for future astronomical instrumentations in space. This allows for mapping more regions of astronomical interest within a space mission lifetime compared to current heterodyne arrays. Similar statements also apply to ground-based telescopes especially at frequencies where suitable weather conditions are rare. The challenge to develop large arrays now is to generate a large LO array with sufficient power and good uniformity among individual beams [11]. In comparison with LO sources based on multipliers [12], quantum cascade lasers (QCLs) are a more promising LO source in the supra-THz region due to its high output power. Current QCLs working at supra-THz frequencies have been demonstrated to cover the range from 1.2 THz to 4.9 THz, and their output powers typically are milliwatts or more [13], which is sufficient as an LO for a heterodyne array with more than 100 mixers. Besides, the distributed-feedback (DFB) laser structures based on double metal waveguide designs allow single-mode emission and high-temperature operation [14]. Therefore, multiplexing a single beam from a QCL by a diffraction grating to generate an LO array is an attractive approach for large heterodyne arrays.

A phase grating has played a crucial role in optics-related science and applications, including orbital angular momentum beams for optical communications, chromatic broadband nulling, UV and terahertz beam multiplexing, and complex beam shaping [15–19]. A phase grating is a periodic structure converting a single coherent radiation beam into multi-beams in different directions by manipulating the phase of the input beam. In [20], Dammann and Görtler proposed gratings with binary groove shapes, called Dammann gratings, and also structures with continuous phase-only groove shapes. Compared to a Dammann grating, a grating with a continuous phase-only groove shape achieves a higher diffraction efficiency, which is defined as the ratio between the power diffracted into the desired orders and the power of the input beam. The use of a Fourier synthesis technique to achieve the continuous phase-only groove shapes was proposed by Schmahl [21], and gratings having a fundamental and a finite number of harmonics are called Fourier gratings [22]. Better milling tool permits fabrication of Fourier gratings with finer features, thus higher diffraction efficiency. In essence, such a structure can also be viewed as a metasurface, manipulating the phase of the incoming beam [23]. Lanigan et al. fabricated a 3-pixel Fourier grating at 0.1 THz [24]. Graf and Heyminck [25] demonstrated an 8 beams grating operated at 490 GHz with a measured diffraction efficiency ~84%. A 7 pixel grating operated at 1.1 THz with diffraction efficiency ~80% has also been realized in [26]. Recently, Mirzaei et al in [27] have pushed the frequency further to 1.4 THz, and even to the 4.7 THz with a 2 × 4 Fourier grating with a diffraction efficiency of 74% in [18]. A 4.7 THz grating of 2 × 4 will be used as an LO multiplexer for mapping [OI] line emission in Galactic/extragalactic Ultra long duration balloon Spectroscopic Stratospheric THz Observatory (GUSTO), which will be launched in 2021 [28]. Fourier gratings have good performance in terms of diffraction efficiency and uniformity among the image beams when the number of output beams is less than 10. In this case, about 20 – 30% of the incoming beam power is diffracted into unwanted higher diffraction order modes. Interestingly, a Fourier grating aiming for more diffraction orders (or

Optics EXPRESS

a large number of diffracted beams) can offer a higher diffraction efficiency according to simulation shown below.

From the manufacturing point of view, accurately duplicating the surface profile of a Fourier grating is crucial [29], especially for large-pixel gratings working at supra-THz regions, since the performance of the grating is dominated by the surface profile. A Fourier grating operated at a higher frequency is more difficult to fabricate since the accuracy is more demanding. In this paper, we present a Fourier grating that generates 81 beams at 3.86 THz, where the incoming beam is provided by an unidirectional antenna coupled 3rd-order distributed feedback (DFB) QCL [30].

2. Fourier grating

2.1. Diffraction theory

Based on the diffraction theory [31], the diffracted far field beam distribution from a phase grating is mathematically represented by

$$U(x,y)=\frac{e^{j\lambda z}}{j\lambda z}e^{j\frac{k}{2z}(x^2+y^2)}\int_{-\infty}^{\infty}\int\{U(\xi,\eta)e^{j\frac{k}{2z}(\xi^2+\eta^2)}\}e^{-j\frac{2\pi}{\lambda z}(x\xi+y\eta)}d\xi d\eta \qquad (1)$$

where the term $U(\xi,\eta)\exp((jk/2z)(\xi^2+\eta^2))$ describes the field distribution in the grating plane. Based on Eq. (1), the far field distribution is the Fourier transform of the field distribution in the grating plane. Since a phase grating manipulates the phase component of the incoming coherent beam, the field distribution in the phase grating plane is $\exp(j\Delta\phi(\xi,\eta))$, where $\Delta\phi(\xi,\eta)$ is called a phase modulation function and is expanded in a Fourier series with a set of Fourier coefficients a_n. Using the Fast Fourier Transform algorithm in Matlab, we define the far field multi-beams distribution. Then a set of a_n is found for the desired number of diffraction orders with high diffraction efficiency and good uniformity using the Standard multidimensional minimization algorithm in Matlab. According to the relation between phase difference and groove depth of the surface structure on the grating $d=\lambda\Delta\phi/4\pi\cos\theta_i$, where λ is the wavelength of the input radiation, $\Delta\phi$ the phase difference, and θ_i the incident angle with respect to the normal direction of the grating, we can define the groove profile of the grating based on the phase modulation function.

2.2. Grating design and fabrication

We generate a two-dimensional (2D) grating by superposition of two 1D gratings orthogonally. Thus its beam pattern is orthogonally distributed. In order to maintain the symmetry, gratings with an even number of employed diffraction-orders (pixels) are added with a half-wave phase step in one half of the unit cell to suppress all the even orders [25], making their surface structure finer than odd-pixel gratings. Besides, even-pixel gratings have lower diffraction efficiency than odd-pixel gratings since the intensities in even diffraction-orders cannot be fully suppressed in most cases. Table 1 shows the diffraction efficiency of 1D gratings with different number of beams and their minimum radius of curvature (MRC) by assuming that the input beam is normally incident to the grating and by assuming a 1.2 mm unit cell. MRC is a crucial parameter for the manufacturer because the designed fine structure of the grating surface can only be reproduced when MRC of the grating is larger than the radius of the ball end mill used in a micro-milling machine. Our initial goal was to demonstrate a 100 beam grating. However, we chose to start with a grating for 81 beams because our simulation shows that a 9 × 9 pixel grating can achieve 98% diffraction efficiency and also a relatively uniform power distribution among the diffracted beams.

Optics EXPRESS

Table 1. The diffraction efficiency and minimum radius of curvature of gratings with different number of beams.*

Pixel number	2	3	4	5	6	7	8	9	10	11
Diffraction efficiency (%)	80.6	92.5	90.8	92.3	86.6	96.9	91.9	99	87.0	97.5
MRC(μm)	102	1167	94	513	84	312	62	267	54	153

*All the gratings are illuminated with a normal incident beam and their unit cell sizes are fixed to 1.2 mm. Generally speaking, odd-pixel gratings have higher diffraction efficiency and larger MRC than what those from even-pixel gratings because even-pixel gratings are added a half-wave phase step in one half of the unit cell.

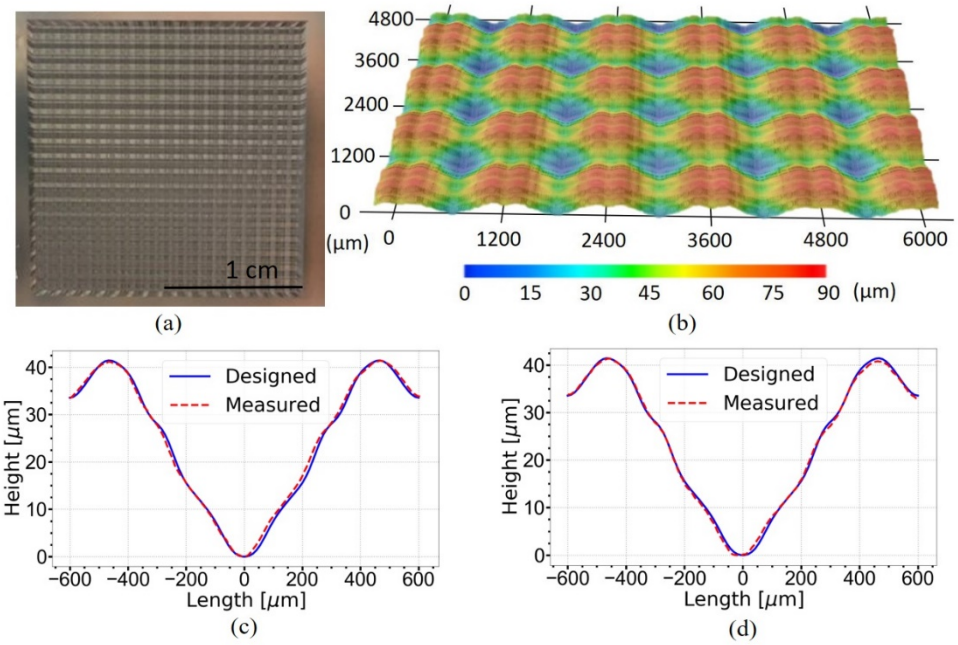

Fig. 1. (a) 81 pixel Fourier grating machined on a 5 mm thick aluminum plate. Gating contains 16 × 16 unit cells, each of them is 1.2 mm × 1.2 mm in size, thus the entire grating is 2 cm × 2 cm. (b) The surface topology of the 81 pixel grating taken by a 3D optical microscope. The color indicates the height. (c), (d) The comparison between the designed profile in red (dashed) and the manufactured profile in blue.

Based on the equation for a 1D reflection grating, $D(\sin\theta_m - \sin\theta_i) = m\lambda$, where D is the periodicity, θ_m is the angle of the m'th diffraction order, and θ_i is the incident angle with respect to the normal of the grating, the angular separation of the image beams is calculated to be ~3.8° (in our case, D = 1.2 mm, θ_i = 12°, and λ = 78 μm). The grating is machined on an aluminum plate (Alcoa QC-10 Mold Alloy, of 5 mm thick) using an KERN EVO micro-milling machine. The MRC for this design is 357 μm, which is about 4 times the radius (90 μm) of the smallest ball end mill currently available for the micro-milling machine used. In this case, this machine is capable of patterning all the fine surface features. A photo of the manufactured grating and its 3D optical microscope image are shown in Fig. 1(a) and (b), respectively. The entire grating contains 16 × 16 unit cells and is 2 cm × 2 cm in size. We also measured the surface profile of a unit cell in two orthogonal directions using a Dektak XT30 stylus profiler. We found good agreement between the measured profile and the designed one with a deviation less than 1 μm in height (1/78 of the working wavelength). The effect of such a difference on the grating performance will be discussed in the results section.

Optics EXPRESS

3. Measurement setup

We apply an unidirectional antenna-coupled 3rd order distributed feedback (DFB) quantum cascade laser (QCL) at 3.86 THz as the input source for the grating. This laser can provide more than 10 mW output power. The unidirectionality, resulting from the reflector shown in Fig. 2(a), enhances the power level of the forward beam by a factor of ~2. In our measurement, we used one of the lasers out of an array of 20 DFB lasers as the input source. Figure 2(b) shows the laser array chip mounted on a carrier.

Figure 3 shows our measurement setup schematically. The QCL was mounted in a pulse tube cooler working at ~10 K. We measured the far field beam pattern of the laser at a distance of about 3.5 cm from the laser, which is shown in Fig. 2(c). The beam has a size ~25 mm in the vertical direction and ~15 mm in the horizontal direction, implying the full width at half-maximum (FWHM) divergence angles to be 23° and 14° in the vertical and horizontal directions, respectively. Obviously the beam has considerable deviation from a fundamental Gaussian beam profile. Since the Fourier grating duplicates the beam pattern of the input beam in its output, directly applying the beam in Fig. 2(c) to the grating requires a large distance to image the output beams with sufficient angular separation to be spatially resolved. However, taking into account the absorption by water vapor in the air at this frequency, we have to choose a short optical path that is within 30 cm in practice. To overcome this issue, we have to make a smaller and collimated incident beam to the grating. We introduced a high-density polyethylene plano-convex lens with a 20 mm focal length to collimate the QCL beam first and then we filtered it with a 5 mm iris aperture. The resulting beam is symmetric and Gaussian-like, shown in Fig. 2(d). This beam is nearly collimated with its FWHM divergence angle to be $< 1°$. It is also important to notice that the incoming beam at the position of the grating has a diameter of 7 mm and covering more than 5 unit cells on the grating. Although the power of the modified beam is lower than the output power of the QCL (5-10% powers), there is still sufficient power to map output beams of the gratings with a good signal-to-noise ratio.

The incident angles of the incoming beam are $12 \pm 2°$ and $\pm 2°$ with respect to the normal of the grating plane in the horizontal and vertical directions, respectively (see Fig. 3). A pyro-electric room temperature detector mounted on a 2D scanner is used to map the image beam pattern at a distance of 12 cm from the grating surface. The detector has a 2-mm diameter aperture and is mounted inside an aluminum housing. The latter together with the planar mapping makes the measured power direction dependent with the maximum if the radiation is incident normally. The detector is read out by a lock-in amplifier. An arbitrary waveform generator is used to modulate the power supplier of the QCL and provides a reference to the lock-in amplifier with a 70 Hz sinusoidal function. A PC is used to control the 2D scanner and record the data from the lock-in amplifier.

To compare the total power of the image beams of the desired modes with that of the input beam, we measured the input beam power in the following way, where the grating is replaced by a gold coated mirror, which reflects nearly 100% power. The reflected single beam is also mapped by the pyro-electric detector at the same distance as measuring the grating imaging beam (12 cm). In this way, we can compare the relative power values accurately since the effect of water absorption due to the optical path is canceled out even though we do not know the absolute power. Caution has been taken to reduce stray light by introducing THz blackbody absorbers to cover the outside area of the circular aperture and the unilluminated area of the grating.

Optics EXPRESS

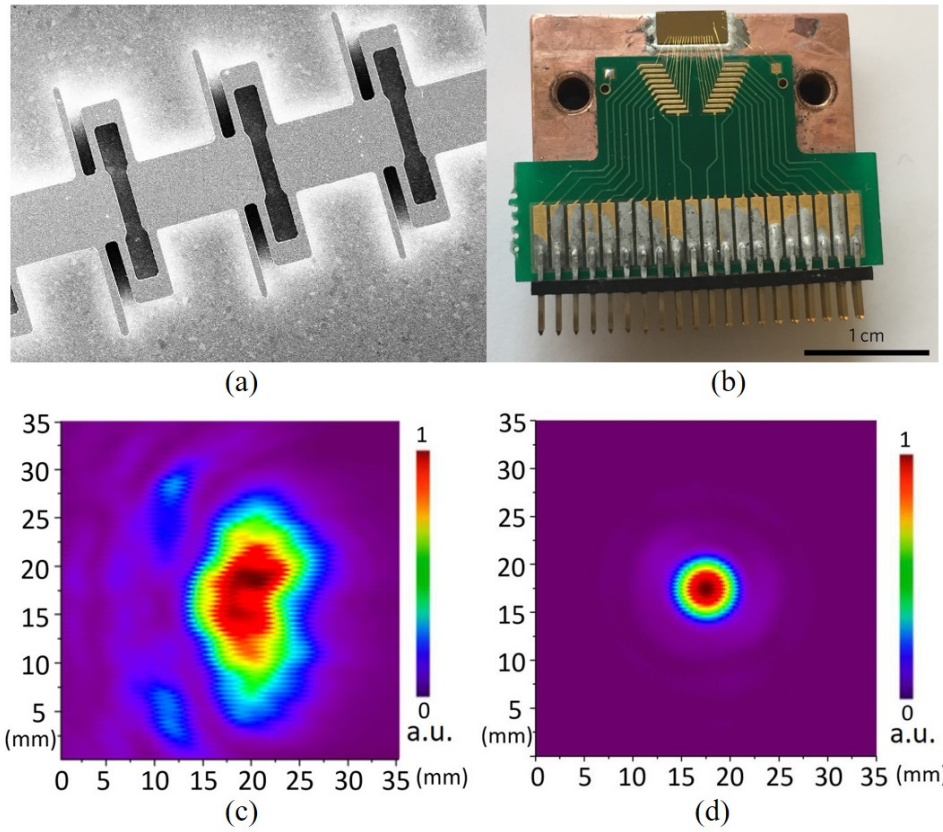

Fig. 2. (a) The SEM of the 3rd-order DFB QCL [30]. (b) Array of DFB lasers gold-wire bonded to an electronic chip [30]. (c) Beam pattern of the QCL measured at a distance ~3.5 cm from the laser. It deviates from Gaussian profile and has large divergence angles in both vertical and horizontal directions. (d) Pattern of the QCL beam collimated by a lens and filtered by an iris aperture, measured after reflection from a flat gold-coated mirror in place of the grating in the setup.

Optics EXPRESS

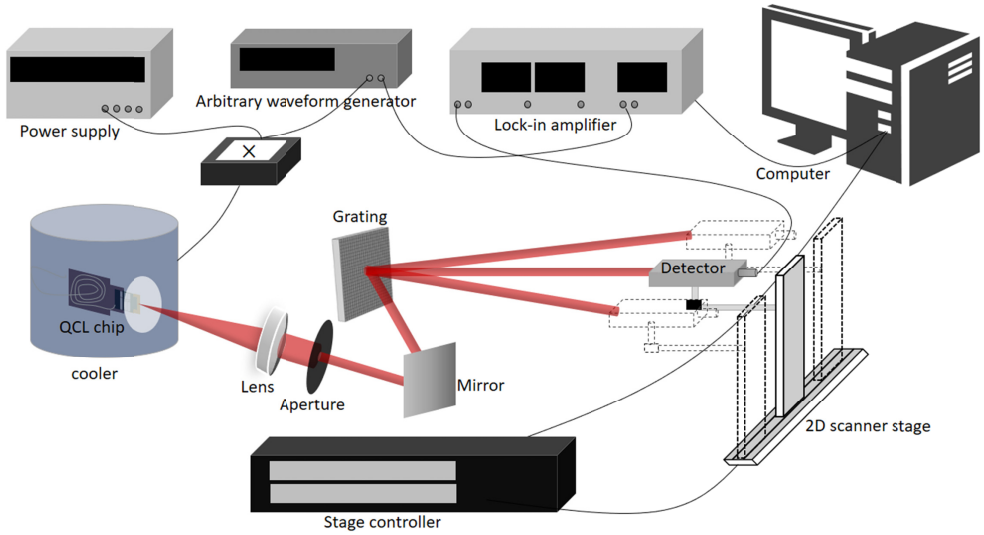

Fig. 3. Schematic diagram of the measurement setup to test the performance of the grating. The QCL is cooled to ~10 K by a pulse tube cooler and its bias voltage is modulated by a sinusoidal function at 70 Hz using an arbitrary waveform generator. The QCL beam is first collimated by a high-density polyethylene lens and filtered by an iris aperture, then reflected by an aluminum mirror to illuminate the grating plane. A pyro-electric detector mounted on a 2D scanner stage is used to map the beam pattern. The received signal is read out by a lock-in amplifier with a 70 Hz sinusoidal function reference. The computer controls the stage and reads out the signal received from the lock-in amplifier.

4. Experiment results and discussions

Figure 4(a) shows our measured beam pattern in a plane with an area of 84 × 84 mm^2, at a distance of 120 mm from the grating surface. The intensity is expressed in units of voltage since the pyro-electric detector converts the detected intensity to voltage. We observed 81 beams, which are well separated, and have angular directions matching to the 1D grating's equation. We do notice some distortions from a perfect rectangular beam distribution, which is most visible in the rightmost column of the beams. The distortions come from the fact that we recorded the beam pattern from a plane, but the appropriate way is to map the beams across a spherical surface since the diffracted beams propagate spherically in space. To visualize the power distribution of the diffracted beams, a 3D plot is also included in Fig. 4(b). We found that the power distribution in the vertical direction of the measured beams is slightly more uniform than the power distribution in the horizontal direction, except for the rightmost column, where the beams are both non-uniform and weaker. This is caused by the incident angle of 12° in the horizontal direction, but normal in the vertical direction.

To compare the measurement with the prediction, Fig. 4(d) shows the simulated diffracted beam pattern of the grating using COMSOL Multiphysics [32]. The result is simulated by importing the surface profile of the designed unit cell of the grating and by repeating it in both orthogonal directions, while taking the input as a Gaussian beam. The simulated far field beam pattern is also plotted along the plane, which has the same distance to the grating surface as in our experiment. We can clearly see 81 rectangularly distributed beams, similar to the measurement in Fig. 4(a). In other words, the simulated 81 beams well reproduce the measured 81 beams. The detailed comparison between measurement and simulation regarding to diffraction efficiency and power uniformity will be given later. It is worth mentioning that the simulation shows the diffracted individual beams have the same beam profile as the input beam. However, we notice that the uniformity of the simulated 81 beams is better than what is seen in the measurement, especially for the beams in the rightmost column. In this analysis, we applied COMSOL because the Fast Fourier Transform algorithm in Matlab used to

Optics EXPRESS

generate the surface profile is not suitable for generating spatially distributed diffracted beams.

For the non-uniformity in the measured beams, there are a few practical factors in the measurement that can affect the uniformity in the beam distribution: (1) There were humidity changes in the laboratory during the beam mapping, which took roughly 20 hours. During this period, the relative humidity varies between 25% and 45%, which in turn changes the absorption and influences the image beam intensity distribution. (2) Power coupling between the pyro-electric detector and the image beams. During the mapping of the image beams, the measured power is angle-dependent, with more power for the beams in the center, but less power for the outer beams. (3) There are possible errors to determine the exact incident angle. The grating is designed for an incident angle of 12° in one direction and 0° in the orthogonal direction. However, in our experiment, it is problematic to determine the incident angle since THz radiation is invisible. We estimate an error of ± 2° on the incident angles, which can also influence the intensity distribution of the image beams. (4) Different distances between the grating and individual image beams. Since we scan the detector along a plane, the distance between the grating and scanning position for each beam varies and it is larger for the outer beams. A longer distance means more loss due to the air absorption. All these experimental errors can influence the measurement of the grating with regard to the diffraction efficiency and uniformity.

To correct the error due to the angle-dependent power measured by the pyro-electric detector, we calibrated the dependence by changing the facing angle of the detector to the beams in both vertical and horizontal directions. We then adjusted the measured intensity of the beams. We also measured the power loss due to different distances between the grating and individual image beams, and found a maximum loss of 0.8%, which is negligible. Other errors are difficult to correct so the only correction is the angular dependence of the detector power in our data analysis. However, we removed the noise floor caused by the pyro-electric detector itself in the image beam data and in the input beam data. Figure 4(c) shows the corrected measured beam pattern, which agrees better with the simulated one in Fig. 4(d). We then calculated the diffraction efficiency based on the corrected data set. We found that the diffraction efficiency is 94 ± 3%. This efficiency suggests that 94% of power has been transferred from the input beam to the diffracted 81 beams by the grating. Clearly, it is a highly efficient Fourier grating. The error bar accounts mainly for the following two sources: the humidity changes in the laboratory and the ± 2° error in the incident angle.

In running COMSOL Multiphysics, we used the periodic port with periodic boundary conditions in the RF (radio frequency) module to get the simulated diffraction efficiency. The simulated diffraction efficiency of the designed grating is 98%, but as stated in section 3, there is a small mismatch (~1 μm) between the manufactured and designed surface profile. So we also imported the manufactured surface profile into COMSOL and found a diffraction efficiency of 97%. It reduces the efficiency by 1%. This 97% value agrees with the measured value of 94 ± 3% within the margin of error.

Optics EXPRESS

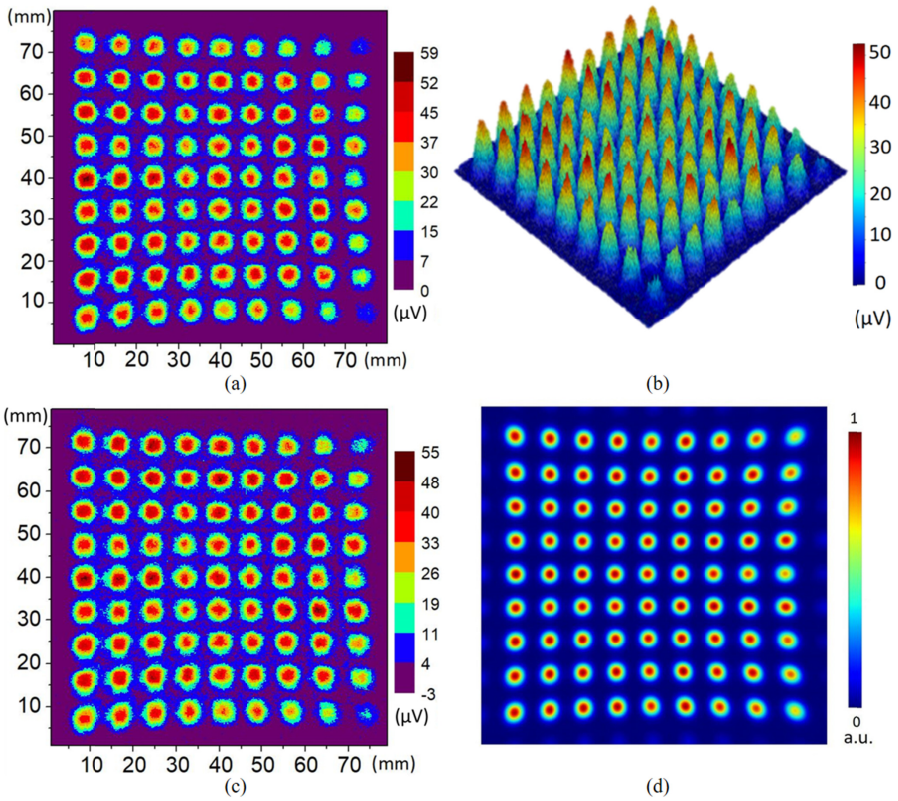

Fig. 4. (a) Measured beam pattern. (b) 3D beam profile of the image beam pattern. (c) Image beam pattern after calibrated the effect of the coupling with detector and removed the noise floor. (d) Simulated far field beam pattern of the designed grating.

Another important performance indicator of a grating is its uniformity in beam power distribution. When the grating is used to generate multiple beams as a local oscillator, each beam will pump a mixer, and thus the power should be within certain range of the desired value, in which all the mixers will perform optimally. The details can depend on the sensitivity of the mixers and the optical components before the mixer. In supra-THz region, superconducting hot electron bolometer (HEB) mixers are the detectors of choice for heterodyne instrumentation due to their high sensitivities and low LO power requirements. However, unlike superconducting–insulator–superconductor (SIS) mixers, which are operated only below 1.4 THz, and Schottky diode mixers, which are relatively insensitive to variation of the LO power, the performance of HEB mixers is LO power dependent [33]. Based on a set of pumped current-voltage characteristic data with a variable LO power in [34] and the isothermal technique [35], we find that if the LO power changes within ± 20% around its optimal power, the receiver noise temperature, which characterizes the sensitivity of a heterodyne receiver, remains at a value within 10% of the best sensitivity [36].

From the data in Fig. 4(c), we calculate the relative power for each beam, and plot them in different columns in Fig. 5(a), where we should expect all the beams to weight for 1.2% of the total power if the diffracted beams are perfectly uniform.

Optics EXPRESS

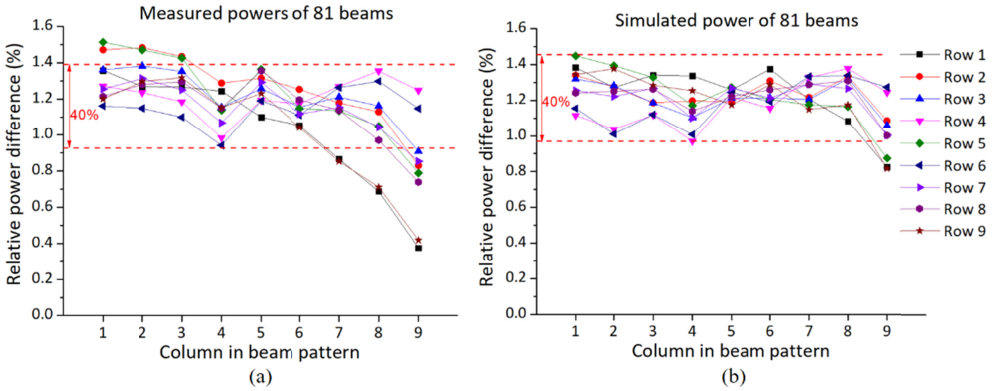

Fig. 5. (a) The power distribution of the measured image beams distributed in different columns. (b) The power distribution of the image beams from the simulation using a designed surface structure.

We found that the relative power varies from 0.4 to 1.5% and the non-uniformity happens mainly on the two rightmost columns (columns 8 & 9) in the measured beam pattern. For comparison, the simulated power distribution is plotted in Fig. 5(b), where the relative power varies from 0.8 to 1.45%. So the simulation gives a better uniformity. However, the simulation also suggests the non-uniformity contributed largely by the rightmost column. From Fig. 5(a) the power of 64 beams out of 81 are within ± 20% range, i.e., the 64 beams can be directly used to pump an uniform HEB mixer array, where every HEB requires the same LO power. In contrast, 78 beams out of 81 vary within this range from the simulation. The difference is likely due to the mismatch between the designed and the manufactured surface profile. By importing one unit cell of the manufactured surface topology into COMSOL Multiphysics and simulating the power distribution of the output beams, we find that 68 beams out of 81 are within ± 20% around the nominal value. Therefore, the precision in manufacturing seems to play a crucial role in the uniformity of the grating. Besides, the humidity change in the laboratory may also affect the uniformity. Despite the non-uniformity in the measured beams, we can still effectively use all 81 beams by replacing the detectors that require lower or higher LO than the nominal value instead of an ideal uniform HEB array. It is relatively easy to control the required LO power of a HEB mixer by controlling the size of an HEB.

To realize the simulated uniformity, we can improve the manufacturing accuracy, for example, to be as good as 0.5 μm. However, to improve the power uniformity of the LO array beyond the current simulation result, there are two possible methods to proceed. Firstly, one can design a 2D grating by directly searching for the Fourier coefficients for a 2D grating instead of superimposing two 1D gratings orthogonally. It has been recently shown that the diffraction efficiency is improved using this method [37]. Potentially it may improve the uniformity, but it needs to be demonstrated in practice. Alternatively, one can use two 1D gratings to generate a rectangularly distributed beam pattern. From the beam pattern in Fig. 4, the power distribution in the vertical direction is obviously more uniform than that in the horizontal direction. That is due to the different incident angles in these two directions, being 0° in vertical direction and 12° in horizontal direction. Illuminating the grating with a normally incident beam will increase the uniformity of the grating, but in reality a non-zero incident angle is needed for a reflection grating. Since both the simulation and measurement results demonstrate that the incident angle in the horizontal direction has nearly no influence on the power uniformity in the vertical direction, one can generate 81 beams by using two separate 1D gratings of 9-pixels in series.

Optics EXPRESS

5. Conclusion

We report a 81-beams supra-THz LO array generated by a Fourier grating with a unidirectional 3rd-order DFB QCL emitting single mode radiation at 3.86 THz. We succeeded in measuring 81 diffraction beams and, due to a high output power of the QCL, we have achieved a good signal-to-noise ratio allowing us to determine the diffraction efficiency of the grating, which is 94 ± 3%, and evaluate the power uniformity of the image beams. The measured diffraction efficiency agrees well with the simulated result using the profile of the manufactured Fourier grating. The latter gives 97% efficiency. Based on the measurements and uniformity requirement of the LO power for superconducting HEB mixers, we find 64 beams out of 81 have their power varying within ± 20% around the nominal value and that the 64 beams can be used to pump a 64 uniform array, maintaining the sensitivity degraded less than 10%. Our results open a new route towards a large heterodyne array of order of 100 pixels for future space instruments. Our Fourier grating approach can improve the functionalities of the phase gratings, such as the diffraction efficiency, for orbital angular momentum beams for optical communications, UV beam splitting, and complex beam shaping.

Funding

China Scholarship Council Studentship (CSC) (201706030153); University of Groningen (RUG); TU Delft Space Institute; National Aeronautics and Space Administration (NASA).

Acknowledgments

We thank Yunchen Luo for developing the grating code, Matt Underhill for fabricating the grating, Marcel Ridder for measuring the grating surface profile, and Paul Urbach for helpful discussions.

References

1. P. Garbacz, "Terahertz imaging – principles, techniques, benefits, and limitations," Problemy Eksploatacji - Maintenance Problems **1**, 81–92 (2016).
2. C. Risacher, R. Güsten, J. Stutzki, H.-W. Hübers, R. Aladro, A. Bell, C. Buchbender, D. Büchel, T. Csengeri, C. Duran, U. U. Graf, R. D. Higgins, C. E. Honingh, K. Jacobs, M. Justen, B. Klein, M. Mertens, Y. Okada, A. Parikka, P. Pütz, N. Reyes, H. Richter, O. Ricken, D. Riquelme, N. Rothbart, N. Schneider, R. Simon, M. Wienold, H. Wiesemeyer, M. Ziebart, P. Fusco, S. Rosner, and B. Wohler, "The upGREAT dual frequency heterodyne arrays for SOFIA," J. Astron. Instrum. **7**(04), 1840014 (2018).
3. C. Pabst, R. Higgins, J. R. Goicoechea, D. Teyssier, O. Berne, E. Chambers, M. Wolfire, S. T. Suri, R. Guesten, J. Stutzki, U. U. Graf, C. Risacher, and A. G. G. M. Tielens, "Disruption of the Orion molecular core 1 by wind from the massive star θ^1 Orionis C," Nature **565**(7741), 618–621 (2019).
4. Y. M. Seo, P. F. Goldsmith, C. Walker, D. J. Hollenbach, M. G. Wolfire, C. Kulesa, V. Tolls, P. N. Bernasconi, Ü. Kavak, F. F. S. van der Tak, R. Shipman, R. G. Jian, A. Tielens, M. G. Burton, H. Yorke, E. Young, W. L. Peters, A. Young, C. Groppi, K. Davis, J. L. Pineda, W. D. Langer, J. H. Kawamura, A. Stark, G. Melnick, D. Rebolledo, G. F. Wong, S. Horiuchi, and T. B. Kuiper, "Probing ISM Structure in Trumpler 14 & Carina I Using The Stratospheric Terahertz Observatory 2," Astrophys. J. **878**(2), 2 (2019).
5. P. H. Siegel and R. J. Dengler, "Terahertz Heterodyne Imaging Part II: Instruments," J. Infrared Millim. Terahertz Waves **27**(5), 631–655 (2006).
6. E. Gerecht, D. Gu, L. You, and K. Sigfrid Yngvesson, "A Passive Heterodyne Hot Electron Bolometer Imager Operating at 850 GHz," IEEE Trans. Microw. Theory Tech. **56**(5), 1083–1091 (2008).
7. S. Kumar, "Recent Progress in Terahertz Quantum Cascade Lasers," IEEE J. Sel. Top. Quantum Electron. **17**(1), 38–47 (2011).
8. U. U. Graf, C. E. Honingh, K. Jacobs, and J. Stutzki, "Terahertz Heterodyne Array Receivers for Astronomy," J. Infrared Millim. Terahertz Waves **36**(10), 896–921 (2015).
9. A. M. Korolev, V. M. Shulga, and S. I. Tarapov, "Extra-low power consumption amplifier based on HEMT in unsaturated mode for use at subkelvin ambient temperatures," Cryogenics **60**, 76–79 (2014).
10. Y. Kim, Y. Zhang, A. Tang, T. Reck, and M.-C. F. Chang, "A 1.5 W 3 GHz Back-End Processor in 65-nm CMOS for Sub-Millimeter-Wave Heterodyne Receiver Arrays," 29th International Symposium for Space Terahertz Technology (ISSTT 2018), pp. 92.
11. J. A. Murphy, C. O'Sullivan, N. Trappe, W. Lanigan, R. Colgan, and S. Withington, "Modal Analysis of the Quasi-Optical Performance of Phase Gratings," J. Infrared Millim. Terahertz Waves **20**(8), 1469–1486 (1999).

Optics EXPRESS

12. J. V. Siles, R. H. Lin, C. Lee, E. Schlecht, A. Maestrini, P. Bruneau, A. Peralta, J. Kloosterman, J. Kawamura, and I. Mehdi, "Development of high-power multi-pixel LO sources at 1.47 THz and 1.9 THz for astrophysics: present and future," 26th International Symposium on Space Terahertz Technology (ISSTT 2015), pp. 40–42.
13. M. S. Vitiello, G. Scalari, B. Williams, and P. De Natale, "Quantum cascade lasers: 20 years of challenges," Opt. Express **23**(4), 5167–5182 (2015).
14. S. Kumar, B. S. Williams, Q. Qin, A. W. M. Lee, Q. Hu, and J. L. Reno, "Surface-emitting distributed feedback terahertz quantum-cascade lasers in metal-metal waveguides," Opt. Express **15**(1), 113–128 (2007).
15. T. Lei, M. Zhang, Y. Li, P. Jia, G. N. Liu, X. Xu, Z. Li, C. Min, J. Lin, C. Yu, H. Niu, and X. Yuan, "Massive individual orbital angular momentum channels for multiplexing enabled by Dammann gratings," Light Sci. Appl. **4**(3), 257 (2015).
16. S. Martin, G. Serabyn, K. Liewer, and B. Mennesson, "Achromatic broadband nulling using a phase grating," Optica **4**(1), 110–113 (2017).
17. Q.-K. Li, Q.-D. Chen, L.-G. Niu, Y.-H. Yu, L. Wang, Y.-L. Sun, and H.-B. Sun, "Sapphire-Based Dammann Gratings for UV Beam Splitting," IEEE Photonics J. **8**(6), 2500208 (2016).
18. B. Mirzaei, J. R. G. Silva, D. Hayton, C. Groppi, T. Y. Kao, Q. Hu, J. L. Reno, and J. R. Gao, "8-beam local oscillator array at 4.7 THz generated by a phase grating and a quantum cascade laser," Opt. Express **25**(24), 29587–29596 (2017).
19. Y. Nakata, K. Osawa, and N. Miyanaga, "Utilization of the high spatial-frequency component in adaptive beam shaping by using a virtual diagonal phase grating," Sci. Rep. **9**(1), 4640 (2019).
20. H. Dammann and K. Görtler, "High-efficiency in-line multiple imaging by means of multiple phase holograms," Opt. Commun. **3**(5), 312–315 (1971).
21. G. Schmahl, "Holographically made diffraction gratings for the visible, UV and soft X-ray region," J. Spectrosc. Soc. Jpn. **23**, 3–11 (1974).
22. P. Bliek, R. Deleuil, M. Breidne, and D. Maystre, "Microwave verification of a numerical optimization of fourier gratings," Appl. Phys. (Berl.) **24**(2), 147–150 (1981).
23. N. Meinzer, W. L. Barnes, and I. R. Hooper, "Plasmonic meta-atoms and metasurfaces," Nat. Photonics **8**(12), 889–898 (2014).
24. W. Lanigan, N. Trappe, J. A. Murphy, R. Colgan, C. O'Sullivan, and S. Withington, "Quasi-optical multiplexing using reflection phase gratings," in 11th International Symposium on Space Terahertz Technology (ISSTT, 2000), pp. 616–625.
25. U. U. Garf and S. Heyminck, "Fourier grating as submillimeter beam splitter," IEEE Trans. Antenn. Propag. **49**(4), 542–543 (2001).
26. C. E. Groppi, C. K. Walker, C. Kulesa, D. Golish, A. Hedden, P. Gensheimer, G. Narayanan, A. W. Lichtenberger, U. U. Graf, and S. Heyminck, "Desert STAR: A 7 pixel 345 GHz heterodyne array receiver for the Heinrich Hertz Telescope," Proc. SPIE **4855**, 330–337 (2003).
27. B. Mirzaei, J. R. G. Silva, Y. C. Luo, X. X. Liu, L. Wei, D. J. Hayton, J. R. Gao, and C. Groppi, "Efficiency of multi-beam Fourier phase gratings at 1.4 THz," Opt. Express **25**(6), 6581–6588 (2017).
28. J. R. G. Silva, B. Mirzaei, W. Laauwen, N. More, A. Young, C. Kulesa, C. Walker, A. Khalatpour, Q. Hu, C. Groppi, and J. R. Gao, "4×2 HEB receiver at 4.7 THz for GUSTO," Proc. SPIE **10708**, 107080Z (2018).
29. H. Dammann and E. Klotz, "Coherent Optical Generation and Inspection of Two-dimensional Periodic Structures," Opt. Acta (Lond.) **24**(4), 505–515 (1977).
30. A. Khalatpour, J. L. Reno, N. P. Kherani, and Q. Hu, "Unidirectional photonic wire laser," Nat. Photonics **11**(9), 555–559 (2017).
31. J. W. Goodman, Introduction to Fourier Optics, (McGraw-Hill, 1968).
32. C O M S O L. Multiphysics, https://www.comsol.com/rf-module.
33. C. E. Groppi and J. H. Kawamura, "Coherent Detector Arrays for Terahertz Astrophysics Applications," IEEE Trans. Terahertz Sci. Technol. **1**(1), 85–96 (2011).
34. P. Khosropanah, J. R. Gao, W. M. Laauwen, and M. Hajeniusb, "Low noise NbN hot electron bolometer mixer at 4.3 THz," Appl. Phys. Lett. **91**(22), 221111 (2007).
35. H. Ekström, B. S. Karasik, E. L. Kollberg, and K. S. Yngvesson, "Conversion gain and noise of niobium superconducting hot-electron-mixers," IEEE Trans. Microw. Theory Tech. **43**(4), 938–947 (1995).
36. The isothermal technique is based on the assumption that the mixer has the same response to LO power and DC power, we can estimate the absorbed LO power in a mixer from the pumped current-voltage curves. In [34] P. Khosropanah, et al measured a set of current-voltage curves of a similar HEB mixer pumped with different LO power operated at 4.3 THz, and from the data when the LO power varies within ~40% the change in HEB mixer's bias current is ~37%, which responds to ~10% changes in the noise temperature.
37. U. U. Graf, "Enhanced diffraction efficiency of two-dimensional phase gratings," Opt. Express **26**(25), 32739–32742 (2018).